Trajectory Dynamics Study of the Ar + CH₄ Dissociation Reaction at High Temperatures: the Importance of Zero-Point-Energy Effects

J. M. C. Marques,*,† E. Martínez-Núñez,‡ A. Fernández-Ramos,‡ and S. A. Vázquez‡

Departamento de Química, Universidade de Coimbra, 3004-535 Coimbra, Portugal, and Departamento de Química Física, Universidad de Santiago de Compostela, Santiago de Compostela E-15782, Spain

Large-scale classical trajectory calculations have been performed to study the reaction $Ar + CH_4 \rightarrow CH_3 + H + Ar$ in the temperature range $2500 \leq T/K \leq 4500$. The potential energy surface used for ArCH₄ is the sum of the nonbonding pairwise potentials of Hase and collaborators (*J. Chem. Phys.* **2001**, *114*, 535) that models the intermolecular interaction and the CH₄ intramolecular potential of Duchovic et al. (*J. Phys. Chem.* **1984**, *88*, 1339), which has been modified to account for the H−H repulsion at small bending angles. The thermal rate coefficient has been calculated, and the zero-point energy (ZPE) of the CH₃ product molecule has been taken into account in the analysis of the results; also, two approaches have been applied for discarding predissociative trajectories. In both cases, good agreement is observed between the experimental and trajectory results after imposing the ZPE of CH₃. The energy-transfer parameters have also been obtained from trajectory calculations and compared with available values estimated from experiment using the master equation formalism; in general, the agreement is good.

1. Introduction

Collision-induced dissociation (CID) processes have long been subject to many studies in various contexts. The CID mechanism may occur through direct dissociation (e.g., as the result of a high energetic collision) where the molecule is fragmented during the initial impact or, in two steps, with the prior formation of an internally excited species followed by its unimolecular dissociation. In both cases, the amount of collisional energy transfer is a key parameter in the study of such reactions. Indeed, knowledge of the mean collisional energy transfer is imperative in using the Rice−Ramsperger−Kassel−Marcus (RRKM) theory[1,2] to calculate rate constants for dissociation (or recombination) reactions. This becomes especially important in combustion chemistry, where the dissociation (or even recombination) reactions occur at high temperatures and low pressures. The RRKM theory uses estimates of the mean collisional energy transfer (which are normally obtained from experimental results on related systems at a particular temperature) to calculate the rate constants for such reactions. Because low-pressure rate constants are quite sensitive to collisional energy transfer, those RRKM calculations may occasionally lead to inaccurate values.

The dissociation reaction

$$M + CH_4 \rightarrow CH_3 + H + M \qquad (1)$$

where M is usually a rare gas atom (e.g., argon), plays a fundamental role in combustion. Under most experimental concentrations of CH₄, reaction 1 can compete with reaction H + CH₄ → CH₃ + H₂, which is clearly important for the CH₄/O₂ combustion chemistry.[3] Because of this, reaction 1 has been

subjected to many experimental[4−9] and theoretical[10,11] studies. Most of these studies focused their attention on the determination (or calculation) of the dissociation rate coefficients in the high-temperature regime. In particular, Kiefer and Kumaran[7] have performed laser-schlieren shock-tube experiments in the temperature range $2800 \leq T/K \leq 4300$ to measure the rate of dissociation of CH₄ diluted in both Ar and Kr. They have concluded that the thermal rate coefficient of reaction 1 should show significant Arrhenius curvature at high temperatures.[7] More recently, Sutherland et al.[12] have used atomic-resonance absorption spectrometry to observe absolute H-atom formation rates from CH₄ dissociation with Kr as a bath gas. These experimental results[12] confirmed those obtained by Kiefer and Kumaran,[7] while establishing that the collisional-energy-transfer parameter in Kr increases with increasing temperature; they[12] expect relatively little difference in the energy-transfer parameter when Kr is replaced by Ar as the bath gas. Moreover, from the theoretical side, Miller et al.[11] have used three formulations of the master equation, applied to methane dissociation in the low-pressure limit, to extract information about collisional energy transfer. Thus, the values of the collisional energy transfer deduced[11] from experimental rate coefficients[7] are shown to increase continuously as the temperature increases from 300 to 4000 K.

The quasi-classical trajectory (QCT) method has proven to be reliable for studying energy transfers in highly excited molecules,[13,14] and, in particular, it has been applied to investigate the energy transfer in collisions of argon with methane.[15−17] However, in comparison with the present work, all of these studies[15−17] have used less realistic analytical models to represent both the intramolecular CH₄ and the intermolecular Ar−CH₄ interactions. Besides, the QCT method has the clear advantage of having no approximation in the dynamics inherent to the energy-transfer process (other than the use of classical mechanics) while allowing the calculation of the relevant parameters without using any kind of experimental data as input.

* Author to whom correspondence should be sent. E-mail: qtmarque@ci.uc.pt.
† Universidade de Coimbra.
‡ Universidad de Santiago de Compostela.

In turn, it also allows the calculation of thermal rate coefficients for reaction 1. Of course, the trajectory approach suffers from some drawbacks, namely, those related to quantum-dynamics effects, and its application to systems with many degrees of freedom is limited by the knowledge of the corresponding potential energy surface and the computational means available. Concerning the quantum effects, one expects tunneling to have a minor influence on the title reaction, once it is barrierless along the minimum energy path. Conversely, as a result of the high endoergicity of reaction 1, the problem of zero-point energy (ZPE) conservation in the CH_3 product should be the most relevant disadvantage of using classical trajectories, even in the combustion range of temperatures. However, many strategies have been proposed[18-35] to approximately correct for this problem. Among these, some are designated as active, because they seek to correct the ZPE leakage along the integration of each trajectory, while the others take into account only the energies of reactant and product molecules (and sometimes that of the transition-state structure) and, hence, are called passive methods. Because the latter do not interfere in the dynamics of the trajectories (they only "manipulate" the statistics of the ensemble of trajectories according to some predefined criteria), they are more convenient from both a practical implementation and theoretical justification; see refs 34 and 36-41 for a critical analysis of the ZPE problem in classical trajectory calculations.

Our main goal is to perform a classical trajectory study of the title reaction in the combustion range of temperatures while assessing the ZPE effects in the thermal rate coefficients; after ZPE correction, the calculated thermal rate coefficients can be compared with the experimental ones. To our knowledge, this is the first theoretical dynamics study attempting to calculate the thermal rate constant for reaction 1. We also want to estimate the Ar + CH_4 collisional energy-transfer parameters at those high temperatures. Thus, the plan of this paper is as follows. In section 2, we give the details about the Ar−CH_4 potential energy surface and describe the process of choosing initial conditions for trajectory calculations. The trajectory analysis (including the way in which the ZPE of CH_3 is imposed) and the results for both thermal rate constants and energy-transfer parameters are presented and discussed in section 3. Finally, section 4 gathers the main conclusions.

2. Trajectory Calculations

2.1. Potential Energy Surface. The potential energy surface for ArCH_4 may be written as

$$V_{ArCH_4} = V_{CH_4} + \sum_{i=1}^{5} V_{Ar-X^i} \tag{2}$$

where V_{CH_4} is the full-dimensional potential function for methane and the five V_{Ar-X^i} (X^1 represents the carbon atom, while X^2, X^3, $X,^4$ and X^5 stand for the hydrogens) pair potentials account for the Ar−CH_4 van der Waals interaction. We have employed the recent intermolecular Ar−CH_4 potential of Hase and collaborators,[42] which is expected to perform well for the range of temperatures studied in this work. This has been calibrated with QCISD(T)/6-311++ G** data,[42] and the corresponding two-body functions have the form

$$V_{Ar-X}(R) = A \exp(-bR) + C/R^6 \tag{3}$$

where the A, b, and C parameters for both Ar−C and Ar−H interactions have been taken from the potential identified as Ar/CH_4−III in ref 42; for other Ar−C and Ar−H potentials,

see refs 43 and 44. The use of eq 3 must be done with some caution for very short Ar−X distances (high energies) where the second term (C is negative) dominates over the first one, which leads to a negative potential. We have verified that those short distances are far from being reached in this trajectory calculation. In addition, the Ar/CH_4−III potential has been shown to provide agreement with high-energy experiments for the Ar + C_2H_6 system.[45]

The potential energy surface adopted in this work for CH_4 is the one of Duchovic, Hase, and Schlegel[46] (DHS), which is known to adequately describe the breakage of the C−H bond, that is, the dissociation reaction $CH_4 \rightarrow CH_3 + H$; this is a key step in the present CID study. However, we have found that the DHS surface allows the H atoms to closely approach each other when CH_4 is highly vibrationally excited, which is not infrequent for the temperatures considered here. Indeed, Hase and collaborators[46] have already pointed out that their CH_4 potential may not be reliable to be used in classical trajectory calculations of methane dissociation at energies where other channels are open [e.g., the reactions $CH_4 \rightarrow CH_2(^1A_1) + H_2$ and $CH_4 \rightarrow CH_2(^3B_1) + H_2$, having thresholds (cf. ref 46) respectively of ∼15 and ∼7 kcal mol^{-1} higher than that for $CH_4 \rightarrow CH_3 + H$]. Thus, we have accounted for the H−H repulsion by adding to the original CH_4 potential six terms of the type
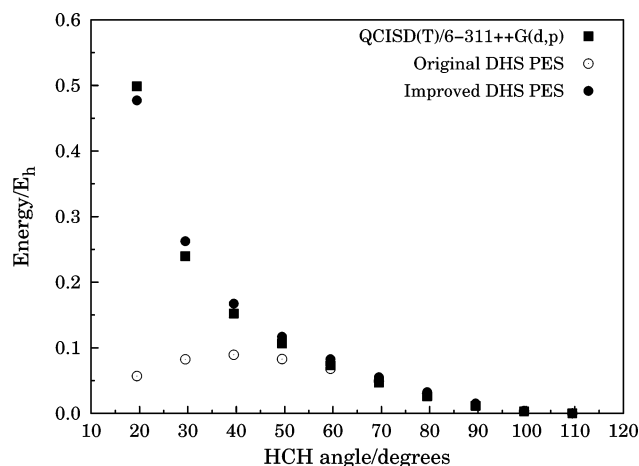
$$V_{H-H}(R) = A \exp(-bR) \tag{4}$$

multiplied by the corresponding switching function

$$f_i(R_{H-H}) = \frac{1}{2}\{1 - \tanh[\gamma(R_{H-H} - R_{cut})]\} \quad (i = 1-6) \tag{5}$$

At small H−H distances (for example, $R_{H-H} < R_{cut}$), the repulsive potential of eq 4 dominates over all of the other CH_4 interactions and disappears for $R_{H-H} > R_{cut}$. We have chosen $R_{cut} = 1.0$ Å because this already corresponds to a strong repulsive interaction region of the DHS surface. Moreover, a rapid switch from the pure repulsive potential given by eq 4 and the DHS function is necessary to reproduce the original CH_4 frequencies at its equilibrium geometry; $\gamma = 100$ Å^{-1} has been found to be a good choice for the decaying parameter of the switching function in eq 5. This new potential function that accounts for the drawback of the DHS surface was then fitted to QCISD(T)/6-311++G(d,p) ab initio points calculated for 10 different HCH angles, and the resulting parameters in eq 4 are $A = 1400$ kcal mol^{-1} and $b = 8.5$ Å^{-1}. Figure 1 shows both the DHS surface[46] and the improved CH_4 potential as functions of the HCH angle. It is clear from this figure that the improved CH_4 surface reproduces quite well the present ab initio calculations, while the DHS one is in complete disagreement for the smallest angles.

Figure 2 shows a contour plot for Ar moving around the CH_4 molecule, which has been fixed at its equilibrium geometry. The topographical details of the intermolecular potential energy surface that stand out in this figure result just from a cut of the global potential energy surface, which corresponds to argon moving in the plane formed by carbon and two of the hydrogen atoms. Because of this, only two of the four equivalent minima ($E_{min} = -0.20$ kcal mol^{-1} below the Ar + CH_4 asymptotic limit) are visible in Figure 2 (shaded areas). These are associated with lines of the Ar−C approach that are perpendicular to the four faces of the tetrahedron, with an argon−carbon distance of $R_{Ar-C} = 4.12$ Å. Also shown by the dots in the figure are two of the saddle points for isomerization ($E_{saddle} = -0.13$ kcal mol^{-1})

Trajectory Dynamics Study of the Ar + CH$_4$ Reaction

J. Phys. Chem. A, Vol. 109, No. 24, 2005 **5417**

Figure 1. Comparisons of the improved DHS potential energy surface (full circles) and the original DHS potential energy surface (open circles) with the QCISD(T)/6-311++G(d,p) ab initio calculations (full squares) as a function of the HCH angle.
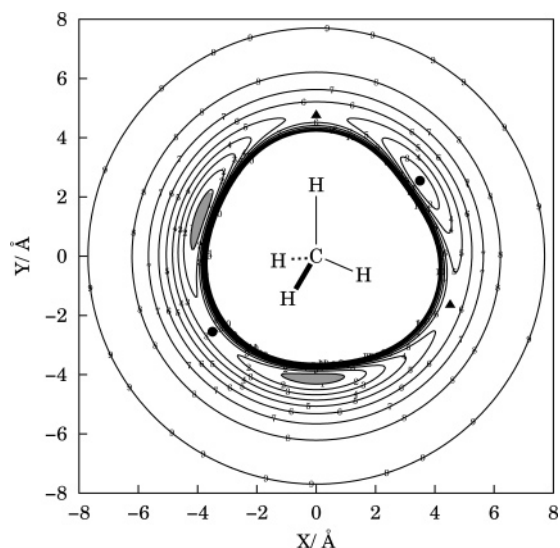
Figure 2. Contour energy plot for the Ar atom around the CH$_4$ molecule (fixed in its equilibrium geometry) in the plane defined by the C−H bonds that are indicated with the thin lines. The C−H bonds standing up and down that plane are represented by the thick and dotted lines, respectively. The first energy contour corresponds to $E_1 = -0.22$ kcal mol^{-1}, $\Delta E = 0.02$ kcal mol^{-1} being the energy difference between contours. The shaded areas show the minima, while full dots and triangles stand for first-order and second-order saddle points, respectively. See the text for further explanation.

that correspond to the edges of the tetrahedron ($R_{Ar-C} = 4.30$ Å); the second-order saddle points ($E_{saddle,2} = -0.07$ kcal mol^{-1}) at the vertices ($R_{Ar-C} = 4.78$ Å) are indicated by triangles in Figure 2. Note that, although deeper (i.e., $E_{min} = -0.39$ kcal mol^{-1}, $E_{saddle} = -0.32$ kcal mol^{-1}, and $E_{saddle,2} = -0.24$ kcal mol^{-1}), similar Ar−CH$_4$ structures ($R_{Ar-C} = 3.70$ Å, $R_{Ar-C} = 3.90$ Å, and $R_{Ar-C} = 4.25$ Å, respectively) have been recently obtained in the CCSD(T)/aug-cc-pVTZ ab initio calculations of Liu and Jäger;[47] these ab initio values are in very good agreement with those from the symmetry-adapted perturbation theory calculations of Heijmen et al.[48]

We present in Figure 3 the main energetic features of the title reaction in the present ArCH$_4$ potential energy surface. It is clear from this figure that the reaction Ar + CH$_4$ → CH$_3$ + H + Ar is highly endoenergetic, with the classical energy threshold being $E_{th} = 110.6$ kcal mol^{-1}. The value of 112.1 kcal mol^{-1} shown in parentheses is estimated from the
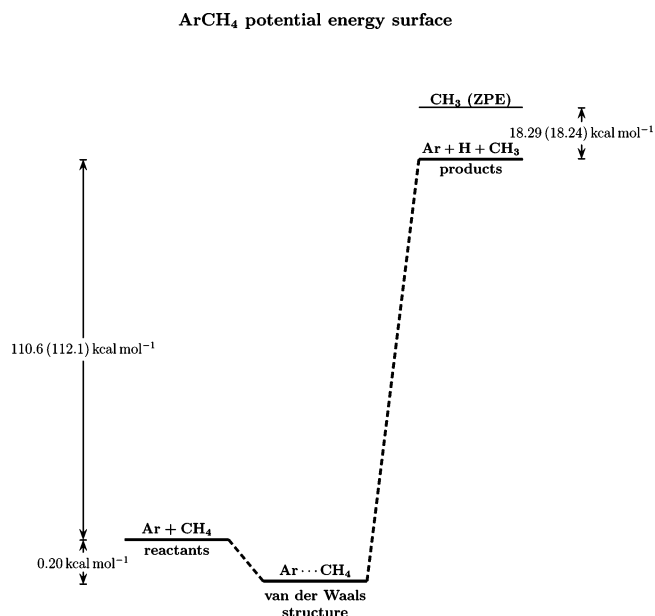
Figure 3. Main energetic features of the reaction Ar + CH$_4$ → CH$_3$ + H + Ar. Values in parentheses are the experimental estimates. See the text for further explanation.

experimental enthalpies at 298.15 K obtained at NIST[49] and taking into account the corresponding thermal energy as well as the ZPEs of both CH$_4$ and CH$_3$. Also indicated in Figure 3 is the Ar−CH$_4$ van der Waals structure associated with the aforementioned four equivalent minima. Finally, we have shown in this figure the ZPE of CH$_3$ (i.e., $E_{ZPE}^{CH_3} = 18.29$ kcal mol^{-1}), which has been calculated using the harmonic frequencies of CH$_3$ arising in a normal-mode analysis of the DHS potential,[46] while the corresponding experimental value is indicated in parentheses.

2.2. Initial Conditions. The thermal rate coefficients were evaluated by the expression[50]

$$k(T) = \left(\frac{8k_BT}{\pi\mu}\right)^{1/2} \sigma(T) \qquad (6)$$

where k_B is the Boltzmann constant, μ is the Ar−CH$_4$ reduced mass, and $\sigma(T)$ is the reactive cross section at temperature T; as usual, $\sigma(T) = \pi b_{max}^2 N_r/N$, with b_{max}, N_r, and N being the largest impact parameter that leads to reaction, the number of reactive trajectories, and the total number of trajectories for a given temperature, respectively. The reactive cross sections have been calculated by running trajectories with an extensively adapted version[44,51,52] of the MERCURY program,[53] which allows for the definition of all possible reactive channels.[44] This has been further modified to incorporate the proper selection of initial conditions for the present work that we describe as follows.

The collision energy E_{tr} has been selected from the Maxwell−Boltzmann distribution at temperature T using the appropriate cumulative function[18]

$$G(E_{tr}) = (k_BT)^{-2} \int_0^{E_{tr}} E'_{tr} \exp(-E'_{tr}/k_BT) \, dE'_{tr} \qquad (7)$$

where the value of E_{tr} for each trajectory is randomly calculated by numerically solving the equation $G(E_{tr}) - \xi = 0$; ξ is a random number chosen in the range $0 \leq \xi \leq 1$. In turn, the vibrational normal modes of CH$_4$ have been sampled quasi-classically from the corresponding Boltzmann distributions, as described in detail in ref 50.

TABLE 1: Trajectory Calculations for the Study of Reaction Ar + CH$_4$ → CH$_3$ + H +Ar^a

T/K	$N_g{}^b$	$f_{ni}{}^c$	T/K	$N_g{}^b$	$f_{ni}{}^c$
2500	6×10^6	0.987	3800	1×10^5	0.740
2800	1×10^6	0.963	4000	4×10^4	0.677
3000	5×10^5	0.936	4200	4×10^4	0.614
3200	5×10^5	0.899	4500	4×10^4	0.524
3500	2.5×10^5	0.827			

^{a} See the text. ^{b} Number of generated trajectories. ^{c} Fraction of the generated trajectories that have been nonintegrated.

The sampling of rotational energy and angular momentum for CH$_4$ takes into account that the molecule is a spherical top with equal momenta of inertia according to the three principal axes of inertia (i.e., $I \equiv I_a = I_b = I_c$). The rotational energy for a spherical top depends only on the rotational angular momentum J (i.e., it has no contribution from the angular momentum component along the molecule-fixed axis) so that J is sampled from the probability distribution

$$P(J) = \frac{J}{Ik_B T} \exp(-J^2/2Ik_B T) \quad (8)$$

where $0 \leq J \leq \infty$ and $P(J)$ is already normalized. Thus, J may be sampled using the cumulative distribution function, which, after integration, leads to the result

$$J = [-2Ik_B T \ln(1 - \xi_1)]^{1/2} \quad (9)$$

Moreover, all three of the components of J are treated on equal footing; that is

$$J_x = J \cos(2\pi\xi_2) \sin(\pi\xi_3) \quad (10)$$

$$J_y = J \sin(2\pi\xi_2) \sin(\pi\xi_3) \quad (11)$$

$$J_z = J \cos(\pi\xi_3) \quad (12)$$

and the classical rotational energy is calculated as $E_{rot} = J^2/2I$; the random numbers ξ_i ($i = 1-3$) belong to the range $0 \leq \xi_i \leq 1$.

Once the initial conditions are established, one of two situations may arise: (i) the total energy ($E_{tot} = E_{vib} + E_{rot} + E_{tr}$) is below the dissociation threshold (i.e., $E_{tot} < E_{th}$), or (ii) $E_{tot} \geq E_{th}$. In case i, the trajectory has no chance of forming products and, hence, it is not integrated, being considered nonreactive. Because of the endoergicity of the reaction, this is the most frequent case, as shown by the fraction of such trajectories in column 3 of Table 1. Thus, from the total number of generated trajectories (N_g) presented in Table 1, only a very small subset (corresponding to those with initial conditions described in case ii) needs to be integrated until one or more internuclear distances reach 10 Å or 90 ps has elapsed. In all cases, the maximum impact parameter (b_{max}) has been fixed at 4 Å. This is well-optimized for the main calculations of the present work, where the ZPE effects have been taken into account (see section 3.1).

Concerning the energy transfer, we have calculated batches of 20 000 trajectories for temperatures $T = 2500, 3000, 3500, 4000,$ and 4500 K. For each batch, the collision energy has been sampled from the corresponding Boltzmann distribution (see above) while the internal energy of CH$_4$ has been fixed at the threshold (i.e., 110.6 kcal mol^{-1}). The rotational counterpart of the latter has been calculated as $RT/2$ (R is the gas constant) for each axis of inertia and the remaining vibrational energy attributed to the normal modes according to a microcanonical

distribution;[54] thus, the initial vibrational (rotational) energies are, in kcal mol^{-1}, 103.2 (7.4), 101.6 (9.0), 100.2 (10.4), 98.7 (11.9), and 97.2 (13.4) for $T = 2500, 3000, 3500, 4000,$ and 4500 K, respectively. The end of trajectories is detected when all of the distances between argon and the other atoms become larger than 15 Å, which is sufficient to ensure that the energy-transfer process is concluded. In turn, b_{max} has been optimized by the procedure of Lim and Gilbert,[55] assuming as criterion of convergence that the second moment of the energy transfer becomes less than 2×10^{-2} cm^{-2} for $b > b_{max}$. Because b_{max} thus calculated should include all of the inelastic collisions, the values obtained are always greater than the corresponding ones for reactive events (i.e., $b_{max} = 4$ Å): $b_{max} = 5.8, 5.6, 5.4, 5.3,$ and 5.4 Å for $T = 2500, 3000, 3500, 4000,$ and 4500 K, respectively. Note that b_{max} is extremely dependent on the potential energy surface; for example, Hase et al.[16] have used $b_{max} = 4.5$ and 5 Å to study the Ar + CH$_4$ collisional energy transfer with different ArCH$_4$ model potentials.

3. Results and Discussion

3.1. Trajectory Analysis. The contribution to the thermal rate constant of the title reaction may arise from (i) the direct formation of Ar + H + CH$_3$ (which is a rare event for endoenergetic processes and has not been observed in the present trajectory calculation), (ii) the formation of a vibrational−rotational excited CH$_4^*$ species (due to collision with Ar) that can dissociate afterward, and (iii) CH$_4^*$ reactants initially prepared with an internal energy above the dissociation threshold. Sometimes the latter should be considered predissociative because they may dissociate prior to the collision with argon. However, a rigorous predissociation criterion cannot be easily established and, hence, it may be assumed that all trajectories initiated with internal energies above the threshold should be discarded from the final statistical analysis; for example, a similar procedure has been adopted by Rodrigues and Varandas[43] in the Ar + HCN collision-induced dissociation. Of course, this criterion for defining predissociative trajectories (hereafter referred to as PD1) should be regarded as an approximation because highly energized CH$_4^*$ species may last for a sufficiently long period so that a collision with argon is able to occur. Besides the PD1 procedure, we have applied the RRKM theory[1,2] to calculate the probability of a trajectory to be predissociative; that is

$$P(t_{col}) = 1 - \exp[-k_{RRKM}(E) \times t_{col}] \quad (13)$$

where $k_{RRKM}(E)$ is the variational RRKM rate constant and t_{col} (=600 ps) is the average collision time calculated by the kinetic theory of gases for the experimental conditions of pressure and temperature adopted by Kiefer and Kumaran;[7] this method of assigning predissociative trajectories will be hereafter referred to as PD2. Although this must still be seen as an approximation, it is clearly a better estimation for predissociative trajectories.

Because the title reaction is highly endoenergetic and the nascent CH$_3$ product molecule has a substantial ZPE content (see Figure 3), we expect that important effects due to ZPE leakage may occur in this system. To investigate this, we have considered three cases in the analysis of the trajectories, those being the results presented in Tables 2−4. First, the pure classical analysis considers that all of the trajectories leading to CH$_4^*$ species with $E_{int} \geq 110.6$ kcal mol^{-1} will promptly dissociate to form H + CH$_3$; the corresponding results are shown in Table 2.

Trajectory Dynamics Study of the Ar + CH$_4$ Reaction

J. Phys. Chem. A, Vol. 109, No. 24, 2005 **5419**

TABLE 2: Results for the Ar + CH$_4$ Reaction Obtained through the Pure Classical Analysis of the Trajectory Calculations and the PD2 Method for Defining Predissociative Trajectories[a]

T/K	N_{tot}	$N_{CH_4^*}$	$10^2\sigma_{CID}/Å^2$	$k(T)/10^9\,cm^3\,s^{-1}\,mol^{-1}$
2500	5 995 964 (5 985 768)	10416 (870)	8.73 ± 0.08 (0.73 ± 0.02)	1130.8 ± 11.1 (94.6 ± 3.2)
2800	996 972 (991 282)	5770 (464)	29.09 ± 0.38 (2.35 ± 0.11)	3987.1 ± 52.3 (322.5 ± 15.0)
3000	496 682 (491 432)	5318 (385)	53.82 ± 0.73 (3.94 ± 0.20)	7635.1 ± 104.1 (558.6 ± 28.5)
3200	493 613 (484 872)	8870 (706)	90.32 ± 0.95 (7.32 ± 0.28)	13234.2 ± 139.2 (1072.4 ± 40.3)
3500	242 764 (234 907)	7929 (593)	164.17 ± 1.81 (12.69 ± 0.52)	25156.6 ± 277.9 (1944.4 ± 79.7)
3800	94 420 (89 664)	4862 (412)	258.83 ± 3.62 (23.10 ± 1.14)	41326.4 ± 577.2 (3687.7 ± 181.3)
4000	36 810 (34 494)	2326 (168)	317.62 ± 6.37 (24.48 ± 1.88)	52030.5 ± 1044.2 (4010.3 ± 308.6)
4200	35 719 (32 928)	2822 (236)	397.12 ± 7.17 (36.03 ± 2.34)	66660.2 ± 1204.2 (6047.2 ± 392.2)
4500	33 723 (30 222)	3544 (280)	528.25 ± 8.39 (46.57 ± 2.77)	91782.1 ± 1458.5 (8091.4 ± 481.3)

[a] Values in parentheses are obtained through the PD1 approach for assigning predissociative trajectories; see the text.

TABLE 3: Results for the Ar + CH$_4$ Reaction Using the "ZPE Analysis" and the PD2 Method for Defining Predissociative Trajectories[a]

T/K	N_{tot}	$N_{CH_4^*}$	N_{600}	N_{diss}	$10^3\sigma_{CID}/Å^2$	$k(T)/10^9\,cm^3\,s^{-1}\,mol^{-1}$
2500	5 998 755 (5 998 724)	105 (88)	33 (31)	17 (16)	0.14 ± 0.03 (0.13 ± 0.03)	1.8 ± 0.4 (1.7 ± 0.4)
2800	998 879 (998 850)	93 (78)	38 (37)	18 (14)	0.90 ± 0.21 (0.70 ± 0.19)	12.4 ± 2.9 (9.7 ± 2.6)
3000	498 576 (498 544)	108 (80)	42 (39)	15 (11)	1.51 ± 0.39 (1.11 ± 0.33)	21.4 ± 5.5 (15.7 ± 4.7)
3200	496 955 (496 903)	213 (183)	63 (59)	36 (35)	3.64 ± 0.61 (3.54 ± 0.60)	53.4 ± 8.9 (51.9 ± 8.8)
3500	246 167 (246 099)	242 (194)	92 (88)	43 (39)	8.78 ± 1.34 (7.97 ± 1.28)	134.5 ± 20.5 (122.1 ± 19.5)
3800	96 850 (96 803)	187 (156)	69 (65)	31 (28)	16.09 ± 2.89 (14.54 ± 2.75)	256.9 ± 46.1 (232.1 ± 43.9)
4000	38 081 (38 061)	103 (91)	39 (38)	20 (18)	26.40 ± 5.90 (23.77 ± 5.60)	432.4 ± 96.7 (389.4 ± 91.8)
4200	37 277 (37 245)	137 (114)	52 (52)	38 (34)	51.24 ± 8.31 (45.89 ± 7.87)	860.1 ± 139.5 (770.2 ± 132.0)
4500	35 786 (35 740)	202 (172)	65 (64)	43 (40)	60.40 ± 9.20 (56.26 ± 8.89)	1049.4 ± 159.9 (977.4 ± 154.5)

[a] Values in parentheses are obtained through the PD1 method for assigning predissociative trajectories; see the text.

TABLE 4: Results for the Ar + CH$_4$ Reaction Using the "ZPE-V Analysis" and the PD2 Method for Defining Predissociative Trajectories[a]

T/K	N_{tot}	$N_{CH_4^*}$	N_{600}	N_{diss}	$10^4\sigma_{CID}/Å^2$	$k(T)/10^9\,cm^3\,s^{-1}\,mol^{-1}$
2500	5 998 755 (5 998 724)	105 (88)	33 (31)	2 (1)	0.17 ± 0.12 (0.08 ± 0.08)	0.2 ± 0.2 (0.1 ± 0.1)
2800	998 879 (998 850)	93 (78)	38 (37)	3 (1)	1.51 ± 0.87 (0.50 ± 0.50)	2.1 ± 1.2 (0.7 ± 0.7)
3000	498 576 (498 544)	108 (80)	42 (39)	3 (3)	3.02 ± 1.75 (3.02 ± 1.75)	4.3 ± 2.5 (4.3 ± 2.5)
3200	496 955 (496 903)	213 (183)	63 (59)	8 (8)	8.09 ± 2.86 (8.09 ± 2.86)	11.9 ± 4.2 (11.9 ± 4.2)
3500	246 167 (246 099)	242 (194)	92 (88)	7 (7)	14.29 ± 5.40 (14.30 ± 5.40)	21.9 ± 8.3 (21.9 ± 8.3)
3800	96 850 (96 803)	187 (156)	69 (65)	6 (6)	31.14 ± 12.71 (31.16 ± 12.72)	49.7 ± 20.3 (49.7 ± 20.3)
4000	38 081 (38 061)	103 (91)	39 (38)	5 (5)	66.00 ± 29.51 (66.03 ± 29.53)	108.1 ± 48.4 (108.2 ± 48.4)
4200	37 277 (37 245)	137 (114)	52 (52)	11 (10)	148.33 ± 44.72 (134.96 ± 42.67)	249.0 ± 75.1 (226.5 ± 71.6)
4500	35 786 (35 740)	202 (172)	65 (64)	12 (11)	168.55 ± 48.65 (154.71 ± 46.64)	292.9 ± 84.5 (268.8 ± 81.0)

[a] Values in parentheses are obtained through the PD1 method of assigning predissociative trajectories; see the text.

In the second approach (hereafter referred to as "ZPE analysis"), all trajectories ending with an internal energy below the ZPE for CH$_3$ (i.e., $E_{int} < 128.89$ kcal mol^{-1}) are considered to be nondissociative. However, because during the dissociation CH$_4^* \rightarrow$ CH$_3$ + H part of the CH$_4^*$ internal energy may be channeled into translation, it is not possible, a priori, to know the number of energized species that will reach a CH$_3$ product with its ZPE. Thus, all trajectories forming CH$_4^*$ species, as defined by the "ZPE analysis", are continued until one of the C–H bonds breaks down (i.e., $R_{C-H} > 10$ Å) or the integration time reaches $t = 600$ ps (i.e., the average collision time estimated for the experimental conditions of Kiefer and Kumaran[7]); the results for the "ZPE analysis" are collected in Table 3. In this table, $N_{CH_4^*}$, N_{600}, and N_{diss} stand for the number of CH$_4^*$ complexes formed in the Ar + CH$_4$ collision, the number of "nondissociating" trajectories, and those leading to CH$_3$ with an internal energy above its ZPE, respectively. Note that the difference between $N_{CH_4^*}$ and $N_{600} + N_{diss}$ corresponds to the number of trajectories dissociating to CH$_3$ without internal energy above the respective ZPE, which are assigned as nonreactive in the "ZPE analysis". In turn, "nondissociating" trajectories correspond to extremely stable CH$_4^*$ species that will last more than the estimated average collision time and, hence, are also considered to be nondissociative. We show in Figure 4 the logarithm of the decay rates for CH$_4^*$ complexes

that follow the PD2 criterion for assigning predissociative trajectories. It is apparent in this figure that the decay rates for $T = 2500$, 3500, and 4500 K present essentially an exponential behavior, although the energy distribution of CH$_4^*$ complexes is far from forming a microcanonical ensemble. Additionally, we have continued the integration after the aforementioned deadline for "nondissociating" trajectories (indicated by the dashed line in Figure 4) up to $t = 9000$ ps and noticed that some CH$_4^*$ complexes dissociate after $t = 600$ ps, but only one forms CH$_3$ with an internal energy above its ZPE for $T = 3500$ K (the same happens for $T = 3200$ and 3800 K, although it is not shown in the figure); for the remaining temperatures, there is no trajectory dissociating with the ZPE of CH$_3$ after $t = 600$ ps. Note also that some CH$_4^*$ complexes do not dissociate even within the long time period of 9000 ps, and they possibly correspond to trajectories with quasi-periodic motion that hardly decay to form products.

Finally, it can be argued that one should look at the vibrational energy rather than the internal energy for comparison with the ZPE of the CH$_3$ product formed in the dissociation of energized CH$_4^*$ species. Accordingly, we have considered a third approach that is similar to the "ZPE analysis" but where the vibrational energy of CH$_3$ substitutes its internal energy in the comparison with the corresponding ZPE; this is hereafter referred to as "ZPE-V analysis", and the main results from this
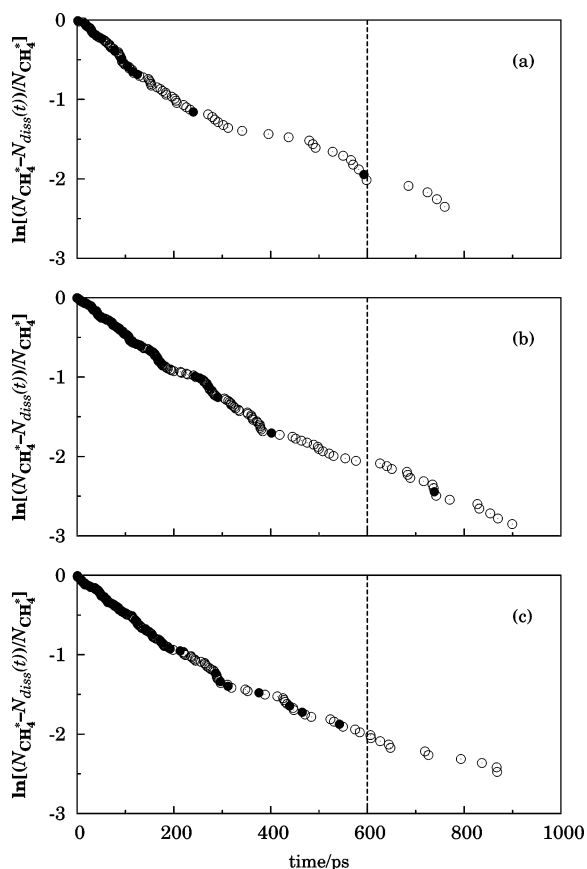
Figure 4. Logarithm of the decay rates as a function of time for the CH_4^* species that fulfill the PD2 criterion for the assignment of predissociative trajectories: (a) $T = 2500$ K; (b) $T = 3500$ K; (c) $T = 4500$ K. Full (open) circles correspond to trajectories that dissociate to form CH_3 with an internal energy above (below) its ZPE. The vertical dashed line sets $t = 600$ ps, which is used to establish the criterion for "nondissociating" trajectories in the present work. Though not shown by the time scale of the figure, trajectories are allowed to dissociate within 9000 ps; after that time, there are 10, 14, and 17 nondissociative trajectories for $T = 2500$, 3500, and 4500 K, respectively. See the text for further explanation.

approach are summarized in Table 4. However, because of vibration–rotation coupling, the corresponding energies are not exactly separable, and it is possible to convert part of one into the other. Note that the final rotational energy ($\langle E_r \rangle$) is calculated in an approximate way by averaging the vibrational motion of the product molecule, and the corresponding vibrational counterpart results from the difference $E_{int} - \langle E_r \rangle$.[53]

The total number of trajectories used in the statistical analysis, which is related to the way of assigning predissociative trajectories (see above), is shown in Tables 2–4 under the symbol N_{tot}. Note that, for each temperature, N_{tot} is smaller when using the PD1 approach for defining predissociative trajectories (values in parentheses) than when using the more accurate PD2 approach considered in this work. The discrepancy between both sets of values is more significant in the case of the pure classical analysis (see Table 2), which may be attributed to its smaller energy threshold in comparison with 128.89 kcal mol^{-1} for the "ZPE analysis" and the "ZPE-V analysis". Of course, a similar trend arises for the number of CH_4^* complexes formed in the Ar + CH$_4$ collision ($N_{CH_4^*}$). Note also that columns corresponding to N_{tot}, $N_{CH_4^*}$, and N_{600} are equal in Tables 3 and 4 because the only difference between the "ZPE analysis" and the "ZPE-V analysis" arises from the type of energy (internal

or vibrational) used for comparison with the ZPE of CH_3 after the dissociation of energized CH_4^* species.

Moreover, we show for completeness, in Tables 2–4, the corresponding values of the CID cross sections (σ_{CID}) and rate constants [$k(T)$]; the latter will be discussed in section 3.2. It is apparent from these tables that, for each temperature, σ_{CID} decreases as the ZPE criterion for trajectory analysis becomes more restrictive. In turn, the values of σ_{CID} tend to increase when using the PD2 assignment of predissociative trajectories despite the PD1 approach (values in parentheses), especially in the cases of classical analysis (Table 2) and "ZPE analysis" (Table 3); for the "ZPE-V analysis" (Table 3), where the number of dissociative trajectories is always very small, σ_{CID} is approximately constant or slightly increases (for $T = 2500$, 2800, 4200, and 4500 K) when passing from PD1 to PD2.

3.2. Thermal Rate Coefficients. One of the main goals of the present work is the study of ZPE effects in the thermal rate constants for the reaction Ar + CH$_4$ → CH$_3$ + H + Ar. For this, we calculated the thermal rate constant as a function of temperature by using the pure classical analysis and two methods for assigning predissociative trajectories, that is, PD1 and PD2 (see section 3.1); the calculated values are shown in column 5 of Table 2. Considering that the experimental values for the rate constant vary from ∼2 × 10^9 cm^3 mol^{-1} s^{-1} at $T = 2500$ K to ∼1 × 10^{12} cm^3 mol^{-1} s^{-1} at $T = 4500$ K, we observe, from Table 2, that the calculated values using the classical analysis of trajectories lead to discrepancies of about 2 orders of magnitude in the case where the PD1 approach has been considered (values given in parentheses); discrepancies of about 3 orders of magnitude are obtained when applying, in contrast, the PD2 method. Although the potential energy surface used here for the ArCH$_4$ species may have some inaccuracies, one can hardly explain such a discrepancy based only on the potential model. In fact, the analytical DHS[46] potential energy surface is expected to describe well the C–H bond rupture, including the angular deformations of both methane and the methyl radical along the minimum energy path. Moreover, as described in section 2.1, we have improved the DHS[46] potential energy surface to eliminate some of its unphysical behavior in describing the H–H repulsion at small internuclear distances; also, the Ar–C and Ar–H pair potentials[42] are expected to be accurate for describing the Ar–CH$_4$ interaction in the range of temperatures considered here. Thus, we believe that ZPE effects have a major influence on the thermal rate constants of the title reaction.

We investigate the importance of ZPE effects in the CH$_3$ product by considering the passive approximations described as the "ZPE analysis" and the "ZPE-V analysis" in section 3.1. We recall here that the "ZPE analysis" considers nonreactive all of the dissociative trajectories forming CH$_3$ products with an internal energy less than its ZPE, while the "ZPE-V analysis" uses, instead, the vibrational energy of CH$_3$ for the same purpose. Note that, for the temperature range considered here, the CH$_4$ reactant is always prepared with an energy content quite above the corresponding ZPE and, hence, is not expected to fall below that value after a nonreactive collision. Because of this, we think that it is useless to apply any ZPE constraint to CH$_4$, as has been done in other works[19,56,57] where the vibrational energy of the reactants is kept constant rather than being randomly selected from appropriate distributions.

The thermal rate constants obtained for reaction Ar + CH$_4$ → CH$_3$ + H + Ar by applying the "ZPE analysis" and excluding the predissociative trajectories identified with the PD2 method are represented in Figure 5. We give in Table 3 the correspond-

Trajectory Dynamics Study of the Ar + CH₄ Reaction

J. Phys. Chem. A, Vol. 109, No. 24, 2005 **5421**
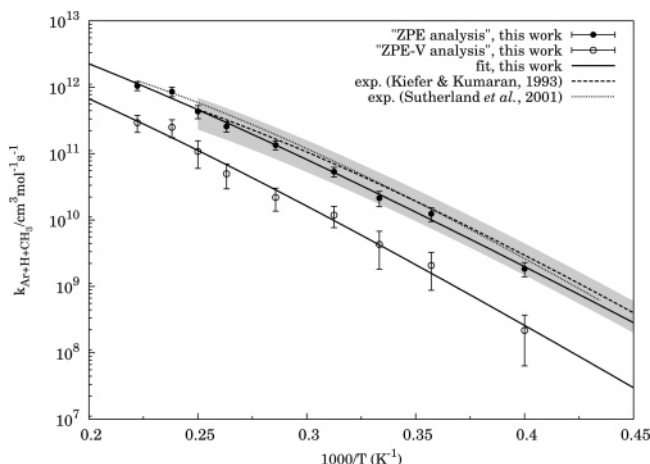
Figure 5. Thermal rate coefficient for the reaction Ar + CH$_4$ → CH$_3$ + H + Ar as a function of temperature. The points refer to the trajectory calculations: "ZPE analysis" (full dots) and "ZPE-V analysis" (open dots). The solid, thick lines correspond to least-squares fits of the calculated points using eq 14; error bars indicate the 68% confidence interval of the Monte Carlo integration. The experimental results are represented by the dashed (ref 11) and dotted (ref 12) lines; the 50% error expected for the experimental results of Kiefer and Kumaran[7] is shown by the shaded area. See the text for further explanation.

ing numerical values as well as those obtained by the PD1 approach (values given in parentheses). It is clear from this table that, in contrast with the pure classical analysis, both PD1 and PD2 approaches give almost the same values for the rate constants. Also shown in Figure 5 are the experimental curves of Kiefer and Kumaran[7] and Sutherland et al.[12] that have been fitted to the generalized Arrhenius expression

$$k(T) = AT^m \exp(-E/RT) \tag{14}$$

where A, m, and E are fitting parameters. Although the experimental results from Sutherland et al.[12] are for the Kr + CH$_4$ reaction, they expect a little difference in the energy transfer for both systems (see also section 3.3) and, hence, the rate constants may be compared with each other. In fact, the values of the rate constants measured by Kiefer and Kumaran[7] and Sutherland et al.[12] agree within ±25% for the temperature range $2300 \leq T/\text{K} \leq 4500$.[12] In turn, the trajectory results arising from the "ZPE analysis" can also be fitted by using eq 14, and the parameters become $\log(A/\text{cm}^3 \text{ mol}^{-1} \text{ s}^{-1}) = 28.7 \pm 13.4$, $m = -3.3 \pm 3.4$, and $E = 92.8 \pm 22.4$ kcal mol^{-1}. Clearly, the agreement between the trajectory results from the "ZPE analysis" and the experiments is quite good, though slightly underestimating them, especially for lower temperatures. Note that even the experimental rate constants are not free from errors, being estimated as ±50% (shaded area in the figure) for the determinations of Kiefer and Kumaran.[7]

Moreover, the rate constants calculated by the "ZPE-V analysis" and using the PD2 approach to identify predissociative trajectories are shown in Figure 5 (open dots), while the numerical values are given in Table 4. Also represented in this table are the corresponding values of $k(T)$ (given in parentheses) obtained by applying the PD1 approach. As in the "ZPE analysis", one can hardly observe significant differences in the values of $k(T)$ obtained by both the PD1 and PD2 approaches. We also show in Figure 5 the curve that fits the values calculated by the "ZPE-V analysis" to eq 14; the fitting parameters are $\log(A/\text{cm}^3 \text{ mol}^{-1} \text{ s}^{-1}) = 29.4 \pm 23.1$, $m = -3.5 \pm 5.8$, and $E = 102.5 \pm 38.6$ kcal mol^{-1}. We observe in Figure 5 that the thermal rate constants from the "ZPE-V analysis" constitute a

lower bound for both the experimental measurements and the values obtained with the "ZPE analysis". This is the expected result because the "ZPE-V analysis" is more restrictive than the "ZPE analysis". Finally, it must be pointed out that, though the "ZPE-V analysis" appears to be more physically acceptable (because one expects the vibrational energy rather than the internal energy to be above the ZPE of CH$_3$), the "ZPE analysis" allows some flexibility in the energy criterion, which perhaps accounts for some lack of accuracy in the calculation of the vibrational energy (see section 3.1); thus, this may explain the good agreement between the values of $k(T)$ calculated from the "ZPE analysis" and those measured experimentally.

3.3. Collisional Energy Transfer. The nth moment of the energy transfer in all of the collisions can be obtained through trajectory calculations by using the expression

$$\langle \Delta E^n \rangle_{\text{traj}} = \sum_{i=1}^{N_{\text{traj}}} \frac{\Delta E_i^n}{N_{\text{traj}}} \tag{15}$$

where N_{traj} is the total number of calculated trajectories for the energy-transfer analysis and ΔE_i is the difference between the initial internal energy of CH$_4$ and its value at the end of trajectory i. Note that eq 15 can be used to calculate the average energy transfer in all collisions ($\langle \Delta E \rangle_{\text{traj}}$) as well as the corresponding root-mean-squared energy ($\langle \Delta E^2 \rangle_{\text{traj}}^{1/2}$). A similar expression also applies for the average energy transfer in deactivating collisions (i.e., trajectories where the internal energy of CH$_4$ diminishes), $\langle \Delta E_d \rangle_{\text{traj}}$. Moreover, it is well-established[13,58−61] that, for a comparison with experimental data, the trajectory results obtained by eq 15 have to be scaled

$$\langle \Delta E^n \rangle = \frac{\pi b_{\text{max}}^2}{\pi \sigma_{\text{LJ}}^2 \Omega^{(2,2)*}} \langle \Delta E^n \rangle_{\text{traj}} \tag{16}$$

where σ_{LJ} is the Lennard-Jones (LJ) collision diameter and $\Omega^{(2,2)*}$ is the LJ collision integral (which can be easily evaluated with the COLRATE code[62]). The standard error of the trajectory results has been estimated by a bootstrap analysis.[63−65]

We show in Figure 6 the values of energy-transfer parameters $\langle \Delta E \rangle$ (panel a), $\langle \Delta E_d \rangle$ (panel b), and $\langle \Delta E^2 \rangle^{1/2}$ (panel c), calculated by scaling the trajectory results (cf. eq 16) for each temperature (T). Also shown in Figure 6 are the recent results of Miller et al.[11] using two different models for the master equation to deduce the energy-transfer parameters from the experimental data of Kiefer and Kumaran.[7] One of these models (hereafter referred to as model I) considers the total energy of CH$_4$ as an independent variable for four different forms of the energy-transfer probability $P(E,E')$ (all shown by the full lines in the figure), while the other (model II) looks at its vibrational energy and uses an exponential form for $P(E,E')$ (dashed lines); see ref 11 for details. Additionally, the $\langle \Delta E \rangle$ values of Sutherland et al.[12] deduced from their experiment on Kr + CH$_4$ (which they expect to be similar to those of Ar + CH$_4$) are also shown in Figure 6a.

From a first glance of Figure 6, we observe that our results are in reasonable agreement with the estimations of Miller et al.[11] and, at least, in qualitative agreement with those of Sutherland et al.[12] for Kr + CH$_4$. In particular, the trajectory results present a good agreement with model I for $\langle \Delta E \rangle$ and $\langle \Delta E^2 \rangle^{1/2}$, while the calculated values of $\langle \Delta E_d \rangle$ overestimate the results of Miller et al.[11] In contrast, our results are in complete disagreement with the energy-transfer values obtained with model II, which has been considered to give too low values.[11]
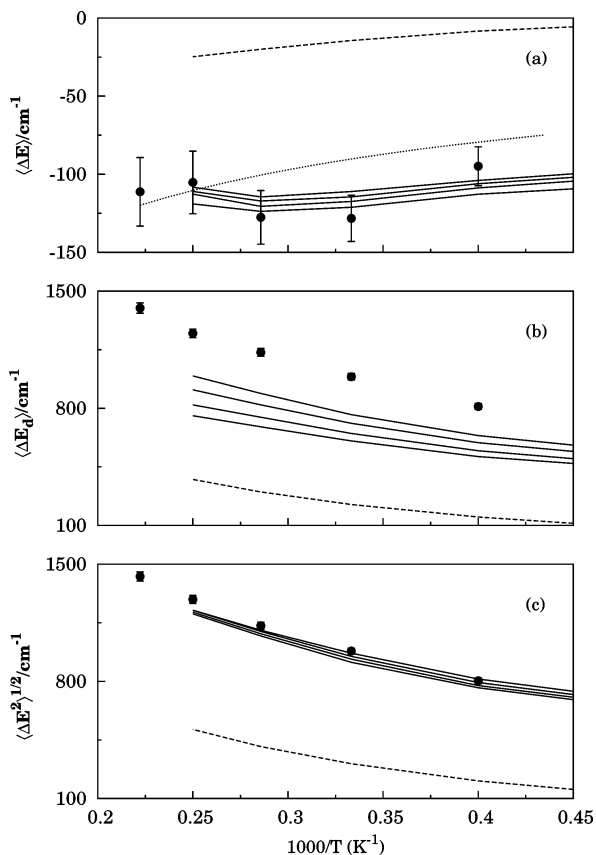
Figure 6. Energy-transfer parameters for Ar + CH$_4$ as a function of temperature: (a) $\langle \Delta E \rangle$; (b) $\langle \Delta E_d \rangle$; (c) $\langle \Delta E^2 \rangle^{1/2}$. The solid dots are the results of the present work obtained from eq 16; error bars are estimated by a bootstrap analysis.[63–65] The results of Miller et al.[11] are represented by the solid and dashed lines; the solid lines correspond to four different forms of the energy-transfer function $P(E,E')$, which depends on the total energy of CH$_4$, while for the results represented in the dashed lines, $P(E,E')$ is an exponential-type function depending on the vibrational energy of CH$_4$. Also shown by the dotted line (panel a) is the result of Sutherland et al.[12] for Kr + CH$_4$. See the text for further explanation.

Another important feature from Figure 6 is that both $\langle \Delta E_d \rangle$ and $\langle \Delta E^2 \rangle^{1/2}$ vary more rapidly with temperature than $\langle \Delta E \rangle$. Thus, as has been advocated by Miller et al.,[11] assuming $\langle \Delta E \rangle$ (despite $\langle \Delta E_d \rangle$) as independent of temperature may be a reasonable first approximation for modeling unimolecular reactions whenever better information is not available. Indeed, though presenting a slightly decreasing tendency (with some oscillations) as T increases, our values of $\langle \Delta E \rangle$ are essentially constant within the error bars (Figure 6a), which is in agreement with the behavior shown by the results of Miller et al.[11] (model I) and, moderately, with those of Sutherland et al.[12] for Kr + CH$_4$.

To gain more insight about the energy-transfer fluxes arising in the trajectory calculations, we have displayed in Figure 7 the average values of energy transfer in all of the collisions from rotation to vibration (R → V′), rotation to translation (R → T′), and vibration to translation (V → T′) as a function of temperature; these values have been calculated on the basis of simple balances among the three types of energy [i.e., vibration (V), rotation (R), and translation (T)], taken on average for the six possible sets in which the trajectories may fall: (i) V activation; (ii) V, T activation; (iii) T activation; (iv) R activation; (v) R, V activation; and (vi) R, T activation. It is clear from Figure 7 that the energy transfer among CH$_4$ internal degrees of freedom ($\langle E_{R\rightarrow V'} \rangle$) is a strong function of temperature
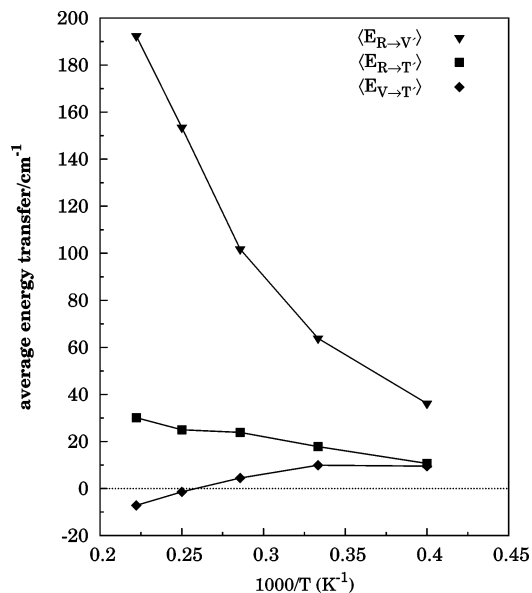
Figure 7. Average values of the energy transfer for rotation to vibration ($\langle E_{R\rightarrow V'} \rangle$), rotation to translation ($\langle E_{R\rightarrow V'} \rangle$), and vibration to translation ($\langle E_{V\rightarrow T'} \rangle$) as a function of temperature: triangles, $\langle E_{R\rightarrow V'} \rangle$; squares, $\langle E_{R\rightarrow T'} \rangle$; diamonds, $\langle E_{V\rightarrow T'} \rangle$. The dotted line is depicted for reference; negative values of the energy transfer mean that the flux is in the reverse direction of the indicated one. See the text for further explanation.

and a significant amount of rotational energy is transferred to vibrational during the inelastic collision process, especially at high temperatures. This may be attributed to a very efficient R−V coupling, which is normally improved as the initial rotational energy is raised, as is the case for increasing temperature (see section 2.2). Clearly, this indicates that rotational degrees of freedom must be treated as active, especially at high temperatures. Conversely, the variations of $\langle E_{R\rightarrow T'} \rangle$ and $\langle E_{V\rightarrow T'} \rangle$ with temperature are, in general, very small. Indeed, $\langle E_{R\rightarrow T'} \rangle$ slightly increases with temperature, while $\langle E_{V\rightarrow T'} \rangle$ appears to decrease at a larger rate (especially for high temperatures), which may be due to a stronger V−T coupling as the collision energy increases (in an average sense) and the vibrational CH$_4$ content decreases (see section 2.2); note also that the V → T′ flux is reversed (i.e., it becomes T → V′) at $T \approx 4000$ K. Because $-\langle \Delta E \rangle$ depends on these two contributions, the reason becomes apparent for its nearly constant value with temperature, as described above (see also Figure 6a).

4. Conclusions

We have performed the first theoretical dynamics study of the Ar + CH$_4$ reaction where the rate constant has been calculated in the temperature range $2500 \leq T/K \leq 4500$. The CH$_4$ DHS surface[46] has been improved by performing QCISD-(T)/6-311++G(d,p) ab initio calculations in order to account for H−H repulsive interactions at high vibrational energies; in addition, the Ar−C and Ar−H pair potentials[42] that have been added to model the Ar−CH$_4$ intermolecular interaction are accurate within the range of temperatures studied in this work. The results show that the ZPE of the CH$_3$ product molecule has a major influence on the calculated thermal rate constants; after ZPE correction, the rate constants present a good agreement with the experimental ones, irrespective of the criterion (PD1 or PD2) used to assign predissociative trajectories. We have also estimated the energy-transfer parameters from trajectory calculations where the initial internal energy of CH$_4$ has been fixed at the dissociation threshold and the collision energy selected from a thermal distribution. The values of $\langle \Delta E \rangle$ and

$\langle \Delta E^2 \rangle^{1/2}$ are in good agreement with those deduced by Miller et al.[11] from the experiment,[7] while overestimating them in the case of $\langle \Delta E_d \rangle$. Finally, we have shown that the nearly constant value of $-\langle \Delta E \rangle$ over the studied range of temperatures results from a subtle balance due to an increase of the average $R \rightarrow T'$ energy transfer and a slightly stronger decrease of the average $V \rightarrow T'$ one.

References and Notes

(1) Marcus, R. A. *J. Chem. Phys.* **1952**, *20*, 359.

(2) Marcus, R. A.; Rice, O. K. *J. Phys. Colloid Chem.* **1951**, *55*, 894.

(3) Warnatz, J. In *Combustion Chemistry*; Gardiner, W. C., Ed.; Springer-Verlag: New York, 1984; p 197.

(4) Roth, P.; Just, T. *Ber. Bunsen-Ges. Phys. Chem.* **1975**, *79*, 682.

(5) Tabayashi, K.; Bauer, S. H. *Combust. Flame* **1979**, *34*, 63.

(6) Klemm, R. B.; Sutherland, J. W.; Rabinowitz, M. J.; Patterson, P. M.; Quartemont, J. M.; Tao, W. *J. Phys. Chem.* **1992**, *96*, 1786.

(7) Kiefer, J. H.; Kumaran, S. S. *J. Phys. Chem.* **1993**, *97*, 414.

(8) Davidson, D. F.; Hanson, R. K.; Bowman, C. T. *Int. J. Chem. Kinet.* **1995**, *27*, 305.

(9) Koike, T.; Kudo, M.; Maeda, I.; Yamada, H. *Int. J. Chem. Kinet.* **2000**, *32*, 1.

(10) Cobos, C. J.; Troe, J. *Z. Phys. Chem. (Muenchen)* **1990**, *167*, 129.

(11) Miller, J. A.; Klippenstein, S. J.; Raffy, C. *J. Phys. Chem. A* **2002**, *106*, 4904.

(12) Sutherland, J. W.; Su, M.-C.; Michael, J. V. *Int. J. Chem. Kinet.* **2001**, *33*, 669.

(13) Brown, N. J.; Miller, J. A. *J. Chem. Phys.* **1984**, *80*, 5568.

(14) Lendvay, G.; Schatz, G. C. In *Classical Trajectory Methods for Studying Energy Transfer from Highly Vibrationally Excited Molecules*; Barker, R. J., Ed.; JAI Press: Greenwich, CT, 1995; Vol. 2B, p 481.

(15) Grinchak, M. B.; Levitsky, A. A.; Polak, L. S.; Umanskii, S. Y. *Chem. Phys.* **1984**, *88*, 365.

(16) Hase, W. L.; Date, N.; Bhuiyan, L. B.; Buckowski, D. G. *J. Phys. Chem.* **1985**, *89*, 2502.

(17) Hu, X.; Hase, W. L. *J. Phys. Chem.* **1988**, *92*, 4040.

(18) Varandas, A. J. C.; Brandão, J.; Pastrana, M. R. *J. Chem. Phys.* **1992**, *96*, 5137.

(19) Varandas, A. J. C.; Marques, J. M. C. *J. Chem. Phys.* **1992**, *97*, 4050.

(20) Marques, J. M. C.; Varandas, A. J. C. *An. Fis.* **1994**, *90*, 284.

(21) Varandas, A. J. C. *J. Chem. Phys.* **1993**, *99*, 1076.

(22) Varandas, A. J. C. *Chem. Phys. Lett.* **1994**, *225*, 18.

(23) Bowman, J. M.; Gadzy, B.; Sun, Q. *J. Chem. Phys.* **1989**, *91*, 2859.

(24) Miller, W. H.; Hase, W. L.; Darling, C. L. *J. Chem. Phys.* **1989**, *91*, 2863.

(25) Varandas, A. J. C.; Marques, J. M. C. *J. Chem. Phys.* **1994**, *100*, 1908.

(26) Ben-Nun, M.; Levine, R. D. *J. Chem. Phys.* **1994**, *101*, 8768.

(27) Kumar, S.; Sathyamurthy, N.; Ramaswamy, R. *J. Chem. Phys.* **1995**, *103*, 6021.

(28) Ben-Nun, M.; Levine, R. D. *J. Chem. Phys.* **1996**, *105*, 8136.

(29) Lim, K. F.; McCormack, D. A. *J. Chem. Phys.* **1995**, *102*, 1705.

(30) McCormack, D. A.; Lim, K. F. *Phys. Chem. Chem. Phys.* **1999**, *1*, 1.

(31) Truhlar, D. G. *J. Phys. Chem.* **1979**, *83*, 18.

(32) Shen, D.; Pritchard, H. O. *J. Chem. Soc., Faraday Trans.* **1996**, *92*, 4357.

(33) Marks, A. J. *J. Chem. Phys.* **1998**, *108*, 1438.

(34) Stock, G.; Müller, U. *J. Chem. Phys.* **1999**, *111*, 65.

(35) Müller, U.; Stock, G. *J. Chem. Phys.* **1999**, *111*, 77.

(36) Lim, K. F. *J. Chem. Phys., Faraday Trans.* **1997**, *93*, 669.

(37) Schlier, C. *J. Chem. Phys.* **1995**, *103*, 1989.

(38) McCormack, D. A.; Lim, K. F. *J. Chem. Phys.* **1995**, *103*, 1991.

(39) Shen, D.; Chan, W.-T.; Pritchard, H. O. *J. Chem. Soc., Faraday Trans.* **1995**, *91*, 3747.

(40) Guo, Y.; Thompson, D. L.; Sewell, T. D. *J. Chem. Phys.* **1996**, *104*, 576.

(41) Peslherbe, G. H.; Hase, W. L. *J. Chem. Phys.* **1996**, *104*, 9445.

(42) Sun, L.; Claire, P. S.; Meroueh, O.; Hase, W. L. *J. Chem. Phys.* **2001**, *114*, 535.

(43) Rodrigues, S. P. J.; Varandas, A. J. C. *J. Phys. Chem. A* **1998**, *102*, 6266.

(44) Varandas, A. J. C.; Pais, A. A. C. C.; Marques, J. M. C.; Wang, W. *Chem. Phys. Lett.* **1996**, *249*, 264.

(45) Brunsvold, A. L.; Garton, D. J.; Minton, T. K.; Troya, D.; Schatz, G. C. *J. Chem. Phys.* **2004**, *121*, 11702.

(46) Duchovic, R. J.; Hase, W. L.; Schlegel, H. B. *J. Phys. Chem.* **1984**, *88*, 1339.

(47) Liu, Y.; Jäger, W. *J. Chem. Phys.* **2004**, *120*, 9047.

(48) Heijmen, T. G. A.; Korona, T.; Moszynski, R.; Wormer, P. E. S.; van der Avoird, A. *J. Chem. Phys.* **1997**, *107*, 902.

(49) NIST Chemistry WebBook. http://webbook.nist.gov/chemistry/.

(50) Peslherbe, G. H.; Wang, H.; Hase, W. *Adv. Chem. Phys.* **1999**, *105*, 171.

(51) Marques, J. M. C.; Wang, W.; Pais, A. A. C. C.; Varandas, A. J. C. *J. Phys. Chem.* **1996**, *100*, 17513.

(52) Marques, J. M. C.; Varandas, A. J. C. *J. Phys. Chem.* **1997**, *101*, 5168.

(53) Hase, W. L. *MERCURY: A General Monte Carlo Classical Trajectory Computer Program*; QCPE 453, 1983.

(54) Hase, W. L.; Buckowski, D. G. *Chem. Phys. Lett.* **1980**, *74*, 284.

(55) Lim, K. F.; Gilbert, R. G. *J. Phys. Chem.* **1990**, *94*, 72.

(56) Hu, X.; Hase, W. L. *J. Phys. Chem.* **1992**, *96*, 7535.

(57) Troya, D.; Pascual, R. Z.; Garton, D. J.; Minton, T. K.; Schatz, G. C. *J. Phys. Chem. A* **2003**, *107*, 7161.

(58) Clarke, D. L.; Oref, I.; Gilbert, R. G.; Lim, K. F. *J. Chem. Phys.* **1992**, *96*, 5983.

(59) Lim, K. F. *J. Chem. Phys.* **1994**, *100*, 7385.

(60) Lim, K. F. *J. Chem. Phys.* **1994**, *101*, 8756.

(61) Lenzer, T.; Luther, K. *J. Chem. Phys.* **1996**, *105*, 10944.

(62) Lim, K. F. *QCPE Bull.* **1994**, *14*, 3.

(63) Efron, B. *SIAM Rev.* **1979**, *21*, 460.

(64) Diaconis, P.; Efron, B. *Sci. Am.* **1983**, *248*, 96.

(65) Lim, K. F. *PEERAN: P(E,E') Error Analysis Program*; Deakin University: Geelong, Australia, 1993.